Design of a Compact Proton Beam Energy Modulator for Imaging

Neerja Aggarwal[a,*], Matthew L. Cavuto[a], Melissa Li[a], Nathaniel H. Rodman[a], Alexander H. Slocum[a], Kyung-Wook Jee[b], Hsiao-Ming Lu[b]

[a]*Massachusetts Institute of Technology, 77 Massachusetts Ave, Cambridge, MA 02139, USA*
[b]*Department of Radiation Oncology, Massachusetts General Hospital and Harvard Medical School, 55 Fruit Street, Boston, MA, 02114, USA*

Abstract

Proton beam therapy is the current state of the art for irradiation of cancerous tumors near vital organs. Proton imaging is a new technology that images tumors with the same particle interaction as proton therapy, promising more accurate treatment preparation compared to traditional computerized tomography scans. A specific proton imaging technique in development at Massachusetts General Hospital requires an energy modulator that can fit inside the gantry nozzle. This work presents the design of a compact proton beam energy modulator required for such imaging applications. A combination of steel and lead wedges was used to create a balanced modulation wheel, with an axis of rotation perpendicular to the incident beam. The mechanical design also allows interchangeable discs and precise position control. The modulator design was verified by testing on a proton beam line. The final device achieved a wide range of energy modulation (21 cm water-equivalent thickness) while maintaining a constant exiting beam angular spread meeting device requirements. This compact design facilitates proton imaging to be practically incorporated into future gantry systems, which will advance proton treatment for tumors near vital organs.

Keywords: proton imaging, energy modulator, proton beam, proton therapy, cancer irradiation, range uncertainty

1. Introduction

Proton beam therapy is the preferred radiation treatment method for treating cancers of vital organs such as brain, prostate, and lungs and cancers in pediatric cases. The treatment is executed by delivering protons of specific energies into a patient's body and taking advantage of Bragg peak of protons where the majority of the dose is deposited at a specific depth. This dose distribution provides accurately delivered ionizing radiation to the targeted tissue while leaving nearby healthy tissue minimally damaged [1]. For treatment planning, the patient's tumor and surrounding anatomy are imaged and modeled through the use of a computerized tomography (CT) scan. Relative proton stopping power of different tissues are also estimated from CT Hounsfield units (HU). As an x-ray based imaging technique, a CT scan uses photons to interact with the patient body's tissue and create an image. However, photons interact with the tissue in a fundamentally different way than protons. Therefore, the deduction of the tissue's proton stopping power from a CT scan has some inherent uncertainty. To account for this uncertainty, clinicians err on the side of caution and treat a larger volume than the tumor itself, thereby damaging surrounding healthy tissue [2].

*Corresponding Author: neerja@alum.mit.edu

[1]Please cite this article as: N. Aggarwal, M.L. Cavuto, M. Li et al., Design of a compact proton beam energy modulator for imaging, Nuclear Inst. and Methods in Physics Research, A (2019) 163269, https://doi.org/10.1016/j.nima.2019.163269.

1.1. Proton Imaging

Many researchers are working to image the patient with the proton beam itself, using the same beam for both imaging and treatment, and minimizing radiation damage to surrounding tissue with range verification using proton radiography (pRG) and proton computed tomography (pCT) [3, 4, 5, 6].

Researchers at Massachusetts General Hospital (MGH) are pursuing specific pRG technique for range verification. In this technique, a time-varying broad energy proton beam is passed through a patient and the dose is recorded on a flat detector as a function of time. To do this, a fixed energy proton beam first passes through a compact energy modulator to create a beam with time-varying energy. As this modulated beam further passes through the patient, it loses energy depending on the thickness and composition of the material in its path. The beam then passes through a silicon flat panel dose detector that measures the dose versus time. This dosage function can be used to calculate the relative stopping power (RSP) of the patient along the beam recorded as the water equivalent path length (WEPL). With a two-dimensional grid of such detectors, a 2-D WEPL image of the patient can be reconstructed, as represented in Figure 1 [7, 8]. Taking the 2-D image from multiple angles can be used to reconstruct a 3-D sectioned image stack of the patient as in pCT. This WEPL image can then be used to develop a more accurate estimation of proton range for a patient treatment with reduced damage to healthy tissue. This optimized curve can be used on xray-CT images for improved conversion of HU to RSP and reduced damage to healthy tissue [9, 10, 11, 12].

The proof of principle of pRG and pCT for range verification on phantoms has been demonstrated [9]. Imaging with

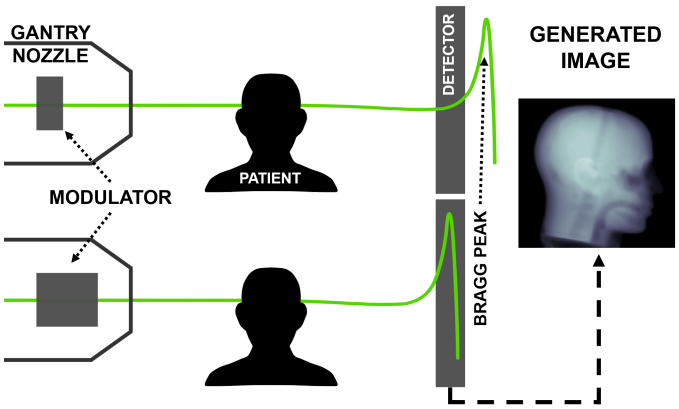

Figure 1: A new proton radiography technique in development at MGH requires an energy modulator that can fit in the gantry nozzle. The modulator sweeps the energy of the beam, which passes through the patient and is measured by a detector. The dose at the detector pixel reaches a maximum when the Bragg peak lands on it. The dosage function at each pixel is used to verify the WEPL and create a image.

proton particles is an active research area and clinical validations are yet to be performed before translating pRG or pCT to clinical use.

A significant challenge in bringing proton imaging to clinical use is incorporating the required hardware into the next generation of proton systems. The pRG technique at MGH requires an extra beam energy modulator that does not currently exist in clinical proton systems.

1.2. Modulator Specifications

Thus, the focus of this work is to design a compact energy modulator that can fit into compact proton systems and support future proton imaging. Lately proton vendors are focusing on creating more compact machines with the pencil beam scanning delivery technique and an option of high energy proton imaging mode. Thus, the modulator was designed based on the following specifications:

1. **Modulation period**: Ideally, proton imaging would be applicable to any part of the body and has the potential to locate a moving target such as lung tumors. To support research in this direction, the device must modulate the beam energy through the entire specified modulation range in under 300 ms. This fast period mitigates motion artifacts in the acquired image due to the patient breathing.
2. **Compact size**: Current energy selection systems are placed upstream of the treatment gantry, meaning the magnets guiding the beam need to readjust each time the beam energy changes, taking on the order of a few seconds for each adjustment. This process is too slow to meet the imaging period specified above. Instead, a new additional modulator inside of the nozzle is proposed, allowing for a single beam energy to pass through the magnets, after which the beam energy can be modulated as quickly as required for proton imaging. The current state of the art pencil beam scanning systems have tight space for an extra modulator in the nozzle. This places a constrain on the size of the energy modulator. For this work, the size constraint was set to a 15 cm cube.
3. **Energy modulation range**: The modulation range of the modulator will determine the maximum WEPL variation of the imaging object that can be measured. A reasonable delta of 25 cm water-equivalent thickness will allow for imaging most parts of the patients body (head, torso, limbs).
4. **Beam angular spread**: Constant proton beam angular spread over beam energy exiting the modulator is desirable in order to image a large area of the target object throughout the entire energy modulation range.
5. **Treatment mode**: During the actual patient treatment, the modulation device should be inactive and not interfere with the treatment beam. Thus the device requires an operation state where the beam is unobstructed by the modulation device.

1.3. Prior Work

Of the several existing energy modulator designs for therapy, those using rotational actuation are more compact and simpler than those using linear actuation, which involve moving wedges or panels linearly in and out of the beam path [13, 14, 15]. The current prototype modulator at MGH, one of the few designed for imaging, uses a rotating disc with increasing thicknesses of aluminum and lead [8]. The beam passes axially through the modulation disc and the energy is modulated by the thickness of the stopping material. An alternative approach is to pass the beam radially through the rotating disc and have wedges of stopping material, as presented by Pu *et al* [16]. Rotating the modulator wheel with an axis perpendicular versus parallel to the beam path is more efficient and balanced around the center of rotation, allowing the final device size to more easily meet the size requirement. Therefore, we combine this approach with the bimetal idea presented in Jee *et al* [8]. The balanced wheel design presented here is an improvement to the previous devices because it meets all specifications above.

This work presents the detailed design of a new compact proton beam energy modulator, composing a bimetal stack of stainless steel and lead wedges, which spins on an axis perpendicular to the incident beam path. The resulting wheel, along with its multiple previous iterations, was experimentally tested on the patient proton beam line at the MGH Francis H. Burr Proton Therapy Center to measure and verify the achieved energy modulation and angular spread. The final design was shown to achieve the desired range of energy modulation and a sufficiently constant angular spread of particle scattering, while remaining compact enough to be integrated into a scanning beam gantry nozzle. This new design will enable proton imaging on future gantry systems and advance the state of the art treatment of tissues near vital organs.

2. Design

2.1. Overview

The final design is as follows: a disc with solid bimetal (lead-steel) wedges rotates along an axis perpendicular to the beam path as shown in Figure 2. Proper material selection and profile design are critical in reducing the size of modulator while meeting the stopping power and scattering requirements. They are described in Section 2.2 and 2.3. All steel components were machined with computer numerical control tools. The lead wedges were cut out with a water jet and attached to the steel wedges with adhesive. The modulation disk was mounted through direct drive to a high torque and low speed servo motor (Teknic Clear Path Integrated Servo System: CPM-MCVC-2310S-RQN; Shaft Diameter: 0.375 in). The motor and modulation wheel assembly was then combined with a simple mounting base and optical stage for fine height and alignment adjustments.

In addition to meeting the specifications above, the prototype design has the following advantages. The two mirrored wedges allow for balanced vibration-free rotation and low required motor torque. The entire modulation wheel was designed to be modular, composing three main sections: a mounting hub, two custom mirrored modulation wedges, and a top shielding plate. With this modular design, researchers can easily design custom modulation wedges of various profiles to suit their specific needs, quickly swapping them out and aligning them to the modulation wheel with the shoulder bolts and top shielding plate. The shoulder bolt material was selected to match that of the modulation wedges, thus rendering them invisible to the beam and eliminating any disturbances to the resulting energy modulation profile.

2.2. Material Selection

Proton beam kinetic energy is often expressed as range, or the depth at which half the protons have come to rest in a medium, usually water. Range can be approximated from initial energy using the Bragg-Kleeman rule as [17] [2]:

$$R \simeq \alpha E_i^p \tag{1}$$

where α and p are material and energy dependent fitted parameters. For example, a 230 MeV beam has a range of 32 cm in water. As the beam passes through materials that degrade its energy, its range also shortens. The delivered dose is proportional to the energy loss at a given depth. Thus the range is related to the depth of the Bragg peak. As the beam passes through thick material, the shape of the Bragg curve is affected due to range straggling and nuclear interactions [2].

The energy loss and nuclear interactions as protons pass through materials like tissues or metals is similar to passing through a standard reference of water [2]. Thus a material's proton stopping power is expressed in water equivalent thickness (WET). Given a thickness of material, t_m, the WET, or t_{WET}, of that material is the thickness of water with the same stopping power, as depicted in Figure 3. The WET is dependent on the density and the atomic number of the material. It can be calculated using the Bragg-Kleeman thick target approach, although it contains many material-dependent parameters and nonlinearities [18]. Instead, the WET simplifies to a linear relation using the International Atomic Energy Agency (IAEA) approximation [19]:

Material	Material thickness for WET = 25 cm (cm)	Beam angular spread after 5 cm of material (deg)
Lead	**4.46**	**5.302**
Steel	**4.58**	**2.867**
Titanium	7.8	1.928
Aluminum	11.86	1.172
Water	25	0.541
Lung Tissue	85.4	0.553

Table 1: WET and beam angular spread for various materials. Lead and steel require less thickness than other materials considered allowing the device to be more compact. Lead and steel have similar stopping but different scattering properties for protons, allowing them to be used in combination to obtain constant beam angular spread.

$$t_w \simeq t_m \frac{R_w}{R_m} \tag{2}$$

where $\frac{R_w}{R_m}$ is the ratio of the final beam range in water versus material m and hence approximately the stopping power ratio.

As protons pass through material, they are also subject to multiple Coulomb scattering (MCS). These elastic scattering events off atomic nuclei deflect the particles' trajectory. This affects the angular spread of the overall beam, here defined as the full width half maximum (FWHM) angle. As a collimated proton beam with angular spread $\theta_i = 0$ enters the modulator, the material scatters the beam, resulting in an angular spread $\theta_f > 0$ as shown in Figure 3. The distribution of the scattered particles is approximately Gaussian. Scattering power is dependent on the material's properties and thickness. The relationship between the resulting angular spread θ_f and material thickness L can be approximated using Highland's formula [20, 21]:

$$\theta_f = \frac{14.1}{pv} z \sqrt{\frac{L}{L_R}} [1 + \frac{1}{9} \log_{10}(\frac{L}{L_R})] \tag{3}$$

where L_R is a material dependent radiation length and pv, ignoring relativistic effects, is approximated to be twice the kinetic energy of the incident proton, and z is the charge of the proton (+1).

The IAEA and Highland approximations were used to calculate the thickness of various materials for 25 cm WET (t_m) and the corresponding final angular spread (θ_f) after 5 cm of material, shown in Table 1. Table 1 shows lead and steel require less thickness of material for a given WET compared to aluminum used by Jee *et al*, allowing for a more compact device [8]. Since steel is easy to machine and requires only 5 cm thickness to obtain 25 cm WET, it was selected as the main material for energy modulation.

However, using only one material for the device will not satisfy the angular spread requirement. Since scattering power increases with material thickness, the thinner sections of steel will result in a smaller angular spread than the thicker sections

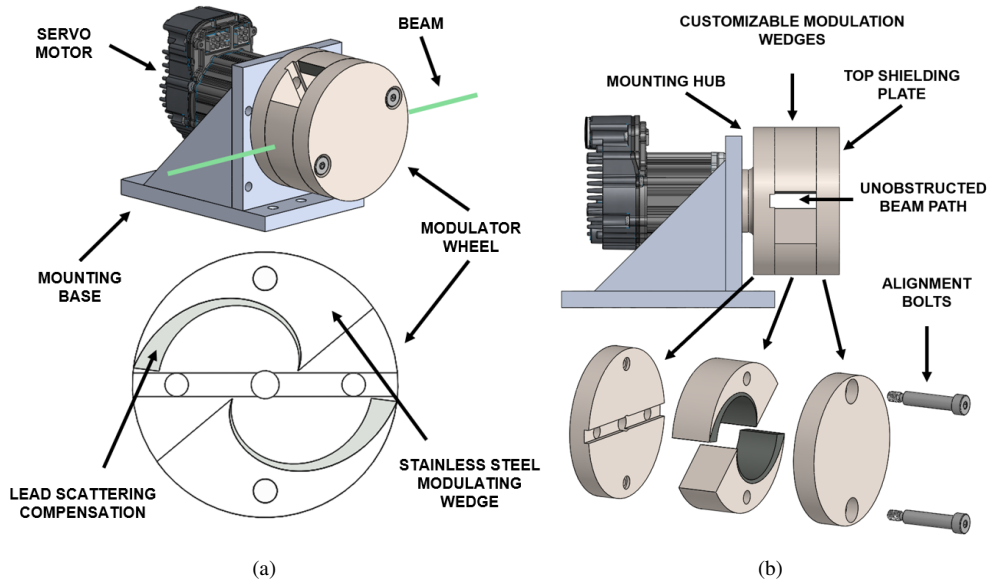

Figure 2: Final proton beam modulator design. The beam direction is depicted in green. (a) Isometric view (top) and cross-sectional view of modulator wheel (bottom). (b) Side view (top) and exploded view showing modulator wheel assembly (bottom).

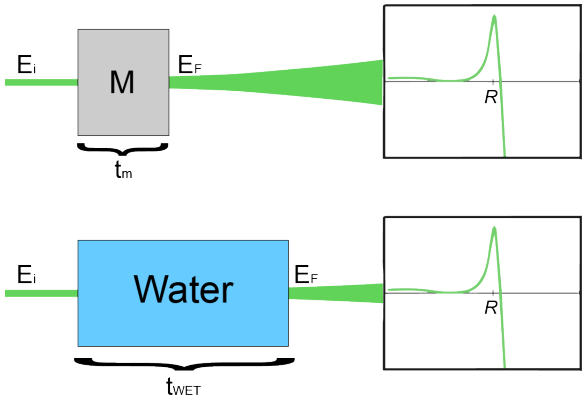

Figure 3: Water equivalent thickness refers to the length the proton must travel in water to achieve the same energy degradation as the material thickness in interest. The resulting beam has the same final energy, E_f, after t_m or t_{WET} but may have differing angular spread.

of steel (Figure 4d). To combat this, a bimetal design is implemented to maintain constant angular spread through the energy modulation range. Table 1 shows lead and stainless steel have similar stopping power but lead has almost double the scattering power. Therefore, a specific combination of the two materials can be used to achieve a desired WET and angular spread. In the final design, as the thickness of steel decreases, the thickness of lead conversely increases.

2.3. Device Profile

The next challenge was designing a device profile using the selected materials. First, the steel wedges were designed to achieve a linear WET increase up to 35 cm WET as the modulator rotated. The following parametric equation driven curve in SOLIDWORKS was drawn as shown in Figure 4:

$$x = (a + \frac{r-a}{\Delta\phi_{range}} * \phi)cos\phi \tag{4}$$

$$y = (a + \frac{r-a}{\Delta\phi_{range}} * \phi)sin\phi \tag{5}$$

where r is the outer diameter of the disk (90 mm), a is the maximum thickness of steel for a single wedge (33 mm), $\Delta\phi_{range}$ is the range of device angle over which the steel thickness increases linearly, and ϕ is the current angle of the device. The axis origin is at the center of the wheel. $\Delta\phi_{range}$ was set to 150° to allow enough room for the 5 mm collimated beam to pass unobstructed through the device during treatment mode. Figure 4 shows using steel only wedges achieves 35 cm WET of stopping power but results in a varying 1-5° angular spread of the final beam.

To calculate the exact profile (thickness versus angle) on the device, a first principles approach was cross-checked with simulation. For the first principles calculation, Highland's formula was numerically evaluated in MATLAB to obtain device angle versus beam angular spread from the steel-only profile achieving 0-35 cm WET. The angular spread from the thickest part of the steel was set to θ_{max}. This is the desired angular spread at all other positions. The angular spread at a given position due to only steel was subtracted from θ_{max}. This angular spread error, $\theta_{max} - \theta(k)$, where k is the position index of the wheel, was interpolated using Highland's formula to calculate the corresponding lead thickness. Thus the original thickness in steel plus the lead compensating thickness should result in constant scattering, θ_{max}, at all positions. The minimum WET obtained was 10 cm (all lead). The maximum WET obtained was 35 cm (all steel). The resulting energy modulation spanned 10-35 cm WET which met the 25 cm WET energy modulation range.

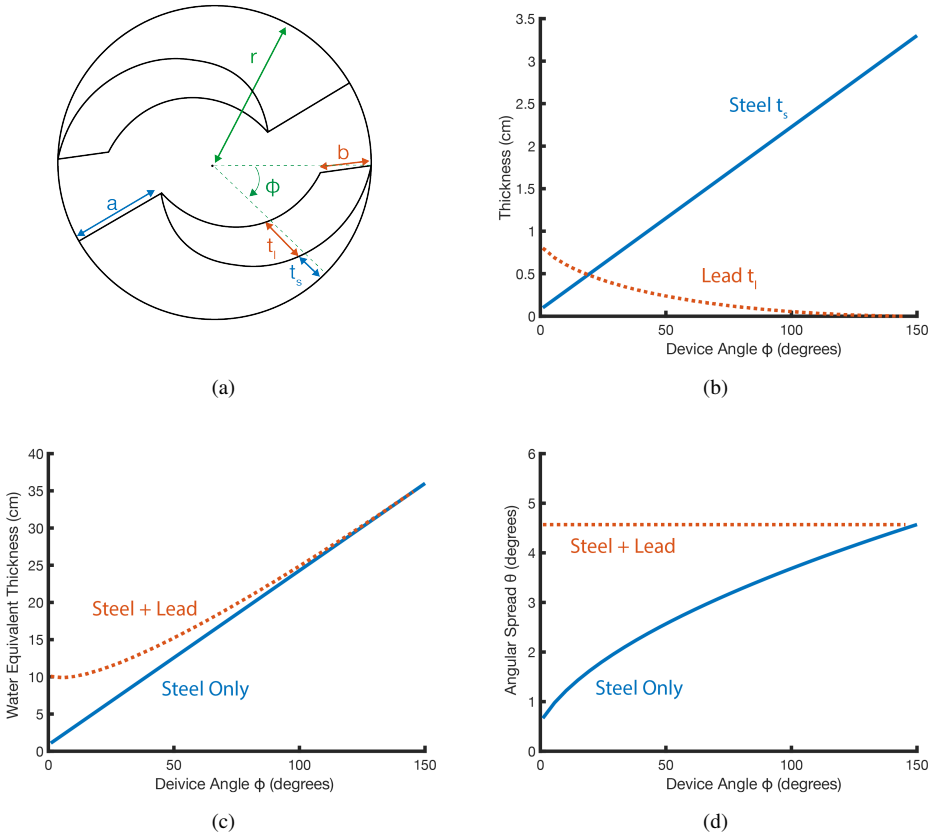

Figure 4: Design calculations for compact proton beam energy modulator. Steel and lead device profile obtains constant beam angular spread over 25 cm WET range of energy modulation. (a) Cross-section of the modulator wheel with lead and steel wedges. The x-axis device angle ϕ goes from the thinnest to thickest part of the wedge. (b) The calculated profile for steel and lead thickness versus device angle for a single wedge. Steel thickness increases linearly with device angle, while lead thickness decreases according to Equation 6. (c) WET versus device angle for steel only and steel plus lead wedges. (d) Beam angular spread versus device angle for steel only and steel plus lead wedges.

The constant angular spread achieved was $\theta_{max} = 2.2°$. Figure 4 shows the expected performance for the final design. The numerically calculated lead thickness versus position graph was fitted to a 3rd-order polynomial to obtain an analytical expression for position versus thickness of lead:

$$t_l = 0.96\theta^3 - 2.5\theta^2 + 3.3\theta - 1 \quad (6)$$

where t_l is the thickness of lead, θ is the device angle of the device (in radians), and the coefficients of the polynomial are from the 3rd-order fit. This expression was used to draw the parametric equation driven curve in SOLIDWORKS for the lead profile.

The calculations using Highland's formula were compared against the angular spread results from LookUp, a FORTRAN based Monte Carlo program written by Gottschalk [21]. The calculations were shown to be within 10-65 percent error of the simulation results.This is because Highland's formula is intended for thin materials. However, Look-Up only allows the angular spread evaluation for a single stack of materials at a time, and is cumbersome when trying to calculate an entire profile of changing material thicknesses. Therefore, our MATLAB script using numerical evaluation of Highland's formula was quicker to use during the preliminary design process of the energy modulator wheel. The parameter inputs of the script could be quickly modified to adjust the energy modulation range and constant angular spread as desired. The result was the approximate bimetal profile needed to achieve the desired energy modulation and angular spread.

The thickness in the radial modulator varies continuously with device angle. In effect, the beam cross-sectional energy at any given instance could be nonuniform depending on the size of the pencil beam. However, the time-resolved proton radiography technique requires the WEPL calibration for every imaging pixel individually. Thus, any spatial variation in energy across the detector will get accounted for during the calibration. Therefore, this nonuniformity should not affect measuring the correct WEPL values for an imaging object.

2.4. Testing and Verification

Experimental testing was conducted at the Francis Burr Proton Therapy Center at MGH on the patient beam lines to verify the design. The collimated proton beam exited the nozzle, passed through the energy modulator, and hit the detector (Figure 5). Two detectors were used during testing at MGH; each detector was placed 75-100 cm from the nozzle.

The Zebra, a multi-layer ion chamber (IBA Dosimetry, Belgium), was used to measure the final beam range and hence en-

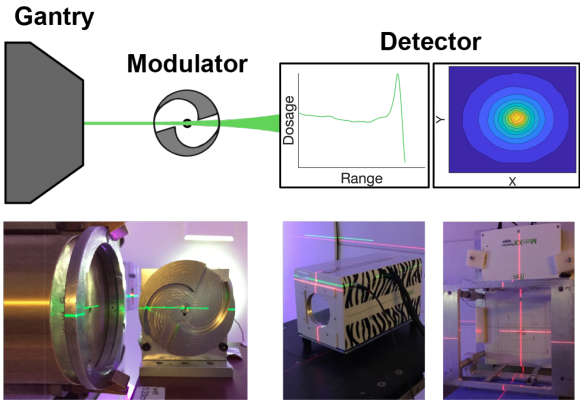

Figure 5: Diagram (top) and images (bottom) of testing setup. The collimated proton beam exited the gantry nozzle, passed through the modulator under test, and hit the detector.

ergy modulation range of the device. The beam passes into the Zebra and through multiple layers of detector plates mimicking 2 mm WET. Each of these plates slightly degrades the energy of the beam and measures the dose applied at that depth. A shifting Bragg peak inside the Zebra indicates changes in the energy of the final modulated proton beam.

The second detector used was the Matrixx (IBA Dosimetry, Belgium) to verify constant angular spread of the final modulated beam. It consists of a matrix of ionization chambers (pixels) to measure dose at different points in the cross-section of the beam. It outputs a 2-dimensional dose plot indicating the spatial distribution of protons hitting the detector.

The modulator was set to rotate at a constant speed of 1 revolution per minute to obtain high resolution data. Because of the double wedge design, this corresponds to two full ranges of energy modulation per minute. With the wheel spinning, a constant stream of protons (233 MeV) was delivered through the device. Each detector was used to collect snapshots of the modulated proton beam's energy span and angular spread at a 1 second time resolution.

3. Results

The testing results confirmed the design calculations and verified that the device met 4 out of 5 of the modulator specifications. The specification not demonstrated was the energy modulation range of 25 cm WET. The energy modulation range demonstrated was 21 cm WET, although the design allows for up to 25 cm WET.

Figure 6 shows the energy modulation range of the device using the measurements from the Zebra detector. As the device rotated, the detector continuously measured the final beam's dosage vs z-depth (as if in water) along the beam axis with an integration time of 1 sec. The data plotted in (a) was smoothed in MATLAB (Savitsky-Golay filter, degree = 1, frame length = 11).

The shifting dosage peak with device angle indicates device was modulating the final beam energy. The unobstructed incident beam at 233 MeV has a range of 32 cm in water. The triple Bragg peak artifact is due to the wide incident beam hitting neither, one, or both of the wedges. As the device angle increases, the Bragg peak jumped to roughly 21 cm in water and was modulated all the way down to 0. Past 0, the Bragg peak did not occur inside the Zebra, but rather inside the modulator wheel. Thus, the true delta of the device is more than 21 cm. The device must be retested with a higher initial proton beam energy above 233 MeV to confirm the stopping power design of 10-35 cm WET which corresponds to a delta of 25 cm WET.

The Matrixx captured the spatial distribution of protons on a plane normal to the beam axis. The xy versus dose data is illustrated as a contour plot in Figure 7a. In order to compare the beam angular spread, the x versus dose data was plotted along y = 0 on the Matrixx and fit to a Gaussian (Figure 7b).

Figure 8 shows the effectiveness of the lead plus steel design. As the beam passed through thicker sections of steel, the dose distribution widened, indicating a slow increase in angular spread for device angles above 0° (Figure 8a). With the added sections of lead, the device is able to maintain a constant FWHM of 16 ± 3 cm for ϕ = 10 to 110 °, as shown in Figure 8a, until the beam is completely blocked. Thus this device maintains constant angular spread.

4. Conclusion

The compact energy modulator prototype demonstrated a delta of 21 cm WET of energy modulation. The device's lead and steel profile achieved a constant angular spread across the energy modulation range. The initial experimental results were first-order consistent with calculations in the design specifications. This compact energy modulator will serve as an essential component of the time-resolved proton radiographic/fluoroscopic imaging technique and will facilitate a practical integration with modern particle therapy systems attributed to its size. Since it is designed to fit directly inside the nozzle of a proton beam line and features both imaging and treatment modes of operation, the acquired beams-eye-view proton images will provide valuable information that improves the therapy target localization as well as reduces the proton range uncertainty. Developmental efforts of utilizing proton imaging to clinical applications will be continued in future studies.

5. Declaration of competing interests

The authors declare that they have no known competing financial interests or personal relationships that could have appeared to influence the work reported in this paper.

6. CRediT authorship contribution statement

Neerja Aggarwal: Conceptualization, Methodology, Writing – original draft, Writing – review & editing. Matthew L. Cavuto: Conceptualization, Methodology, Writing – original draft, Writing – review & editing. Melissa Li: Conceptualization, Methodology, Writing original draft, Writing – review

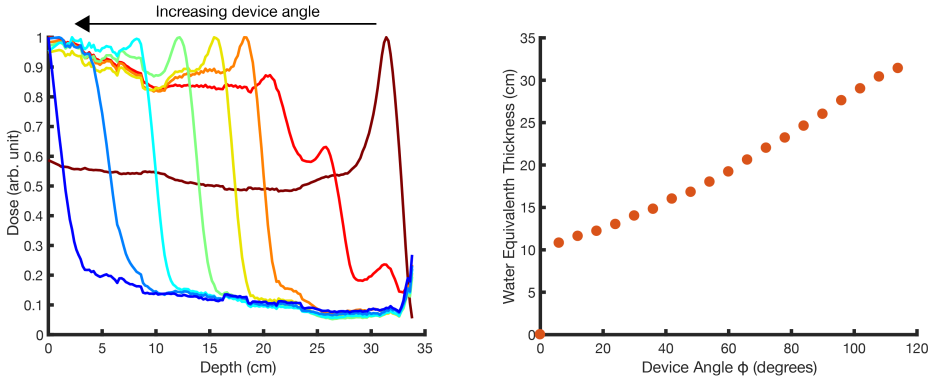

(a) (b)

Figure 6: (a) The z-depth versus dose graph of the final beam energy at increasing device angles measured by a multi-layer ion chamber. The unobstructed proton beam's Bragg peak (far right curve, device angle = 0) is at 32 cm. As the device continuously rotates (0 to 180 degrees) and modulates the energy of the proton beam, the Bragg peak jumps to 21 cm and decreases down to 0. (b) The measured WET versus device angle is plotted using the results in (a). The device was validated only up to 21 cm of WET modulation range due to the limited maximum proton range (32 cm) at MGH.

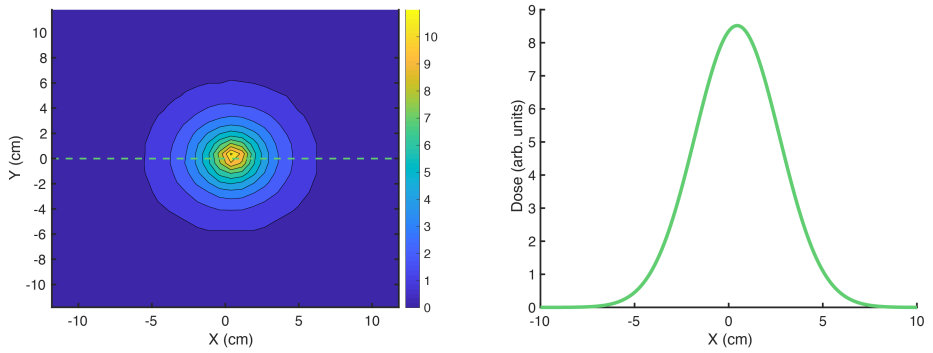

(a) (b)

Figure 7: (a) An example 2-D dose plot from the ionization matrix detector. (b) The dose vs horizontal displacement, x, at y = 0 as a 1-D graph and fit to a Gaussian curve.

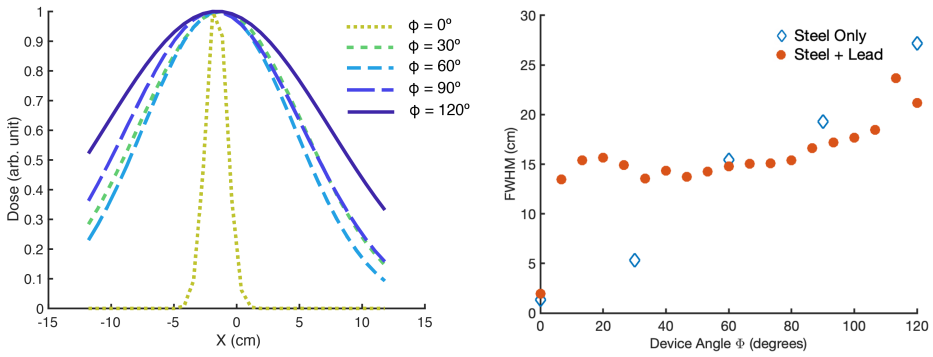

(a) (b)

Figure 8: (a) Dose vs horizontal displacement, x, for the final steel with lead design is plotted at multiple device angles, ϕ. Each curve is used to calculate the full-width-half-maximum (FWHM) for each device angle. (b) The FWHM from the final beam spread is plotted against device angle for both steel only and steel plus lead designs. The FWHM for the improved steel plus lead design stays constant at 16 ± 3 cm for ϕ = 10 to 110 indicating constant scattering.

& editing. Nathaniel H. Rodman: Conceptualization, Methodology. Alexander H. Slocum: Supervision, Conceptualization, Writing – review & editing. Kyung Wook Jee: Conceptualization, Writing – original draft, Writing – review & editing. Hsiao-Ming Lu: Conceptualization, Writing – review & editing.

7. Acknowledgements

The authors would like to thank Dr. Nevan Hanumara and Daniel Teo for technical guidance during the design process. Thank you to the research staff at the MGH Francis H. Burr Proton Beam Therapy Center for assistance with testing of the prototype. This project was part of MIT Course 2.75 Medical Device Design: web.mit.edu/2.75.

8. References

1. Paganetti H. Proton therapy physics. *Health Phys* 2012;103.
2. Newhauser WD, Zhang R. The physics of proton therapy. *Physics in Medicine and Biology* 2015;60(8):R155–209.
3. Schneider U, Besserer J, Pemler P, Dellert M, Moosburger M, Pedroni E, Kaser-Hotz B. First proton radiography of an animal patient. *Med Phys* 2004;31(5):1046–51. doi:10.1118/1.1690713.
4. Schneider U, Pemler P, Besserer J, Pedroni E, Lomax A, Kaser-Hotz B. Patient specific optimization of the relation between CT-Hounsfield units and proton stopping power with proton radiography. *Med Phys* 2005;32(1):195–9. doi:10.1118/1.1833041.
5. Poludniowski G, Allinson NM, Evans PM. Proton radiography and tomography with application to proton therapy. *Br J Radiol* 2015;88(1053):1–14. doi:10.1259/bjr.20150134.
6. Johnson R. Review of medical radiography and tomography with proton beams. *Reports Prog Phys* 2018;81(1). doi:10.1088/1361-6633/aa8b1d.
7. Lu H. A potential method for in vivo range verification in proton therapy treatment. *Physics in Medicine and Biology* 2008;53(5):141324.
8. Jee KW, Zhang R, Bentefour EH, Doolan PJ, Cascio E, Sharp G, Flanz J, Lu HM. Investigation of time-resolved proton radiography using x-ray flat-panel imaging system. *Phys Med Biol* 2017;62(5):1905–19.
9. Testa M, Verburg JM, Rose M, Min CH, Tang S, Bentefour EH, Paganetti H, Lu HM. Proton radiography and proton computed tomography based on time-resolved dose measurements. *Phys Med Biol* 2013;58(April):8215–33. URL: http://www.ncbi.nlm.nih.gov/pubmed/24200989. doi:10.1088/0031-9155/58/22/8215.
10. Bentefour EH, Schnuerer R, Lu HM. Concept of proton radiography using energy resolved dose measurement. *Phys Med Biol* 2016;61(16):N386–93. doi:10.1088/0031-9155/61/16/N386.
11. Zhang R, Jee KW, Cascio E, Sharp GC, Flanz JB, Lu HM. Improvement of single detector proton radiography by incorporating intensity of time-resolved dose rate functions. *Phys Med Biol* 2018;63(1). doi:10.1088/1361-6560/aa9913.
12. Zhang R, Sharp GC, Jee KW, Cascio E, Harms J, Flanz JB, Lu HM. Iterative optimization of relative stopping power by single detector based multi-projection proton radiography. *Phys Med Biol* 2019;64(6). doi:10.1088/1361-6560/aaf976.
13. Fujimaki H, Totake S. Charged particle beam irradiation system. U.S. Patent 7 977 656; July 12, 2011.
14. Guertin T, Marc M. Energy modulator for modulating an energy of a particle beam. U.S. Patent 8 330 132; December 11, 2012.
15. Westerly DC. Scanning aperture ion beam modulator. U.S. Patent 7 977 648; July 12, 2011.
16. Pu Y. Charged particle beam irradiation apparatus and method of irradiation with charged particle beam. U.S. Patent 6 034 377; March 7, 2000.
17. Zhang R, Newhauser WD. Calculation of water equivalent thickness of materials of arbitrary density, elemental composition and thickness in proton beam irradiation. *Physics in Medicine and Biology* 2009;54(6):1383–95.
18. Bragg WH, Kleeman R. XXXIX. On the α particles of radium, and their loss of range in passing through various atoms and molecules . *The London, Edinburgh, and Dublin Philosophical Magazine and Journal of Science* 1905;10(57):318–40. doi:10.1080/14786440509463378.
19. Absorbed dose determination in external beam radiotherapy. Tech. Rep.; IAEA Technical Report Series No 398 (Vienna: International Atomic Energy Agency); 2000.
20. Highland VL. Some practical remarks on multiple scattering. *Nuclear Instruments and Methods* 1975;129:497–9.
21. Gottschalk B. On the scattering power of radiotherapy protons. *Medical Physics* 2010;37(1):352–67. doi:10.1118/1.3264177.